Available online at www.sciencedirect.com

ScienceDirect

www.elsevier.com/locate/jes

JES JOURNAL OF ENVIRONMENTAL SCIENCES

www.jesc.ac.cn

Formation of halonitromethanes from methylamine in the presence of bromide during UV/Cl_2 disinfection

Lin Deng[1], *Wei Luo*[1], *Xiao Chi*[2], *Tingting Huang*[1], *Longjia Wen*[1], *Huiyu Dong*[3], *Mingxian Wu*[4], *Jun Hu*[1,3,4,5,*]

[1] *Department of Municipal Engineering, Southeast University, Nanjing 211189, China*
[2] *Zhejiang Haihe Environmental Technology Co., Ltd., Jinhua 321000, China*
[3] *Research Center for Eco-Environmental Sciences, University of Chinese Academy of Sciences, Chinese Academy of Sciences, Beijing 100085, China*
[4] *Zhejiang Truelove Blanket Technology Co., Ltd., Jinhua 322000, China*
[5] *College of Environment, Zhejiang University of Technology, Hangzhou 310014, China*

ARTICLE INFO

Article history:
Received 3 November 2021
Revised 20 December 2021
Accepted 22 December 2021
Available online 4 January 2022

Keywords:
HNMs
UV/Cl_2 process
Methylamine
Bromide

ABSTRACT

The UV/Cl_2 process is commonly used to achieve a multiple-barrier disinfection and maintain residuals. The study chose methylamine as a precursor to study the formation of high-toxic halonitromethanes (HNMs) in the presence of bromide ions (Br^-) during UV/Cl_2 disinfection. The maximum yield of HNMs increased first and then decreased with increasing concentration of Br^-. An excessively high concentration of Br^- induced the maximum yield of HNMs in advance. The maximum bromine incorporation factor (BIF) increased, while the maximum bromine utilization factor (BUF) decreased with the increase of Br^- concentration. The maximum yield of HNMs decreased as pH value increased from 6.0 to 8.0 due to the deprotonation process. The BUF value remained relatively higher under an acidic condition, while pH value had no evident influence on the BIF value. The maximum yield of HNMs and value of BUF maximized at a Cl_2:Br^- ratio of 12.5, whereas the BIF value remained relatively higher at low Cl_2:Br^- ratios (2.5 and 5). The amino group in methylamine was first halogenated, and then released into solution as inorganic nitrogen by the rupture of C-N bond or transformed to nitro group by oxidation and elimination pathways. The maximum yield of HNMs in real waters was higher than that in pure water due to the high content of dissolved organic carbon. Two real waters were sampled to verify the law of HNMs formation. This study helps to understand the HNMs formation (especially brominated species) when the UV/Cl_2 process is adopted as a disinfection technique.

Introduction

To prevent the spread of disease, free chlorine (Cl_2, HOCl/OCl^-) is widely used as a drinking water disinfectant, which can quickly inactive most of pathogenic microbes. However, chlo-

* Corresponding author.
E-mail: hujun1988@zjut.edu.cn (J. Hu).

https://doi.org/10.1016/j.jes.2021.12.031

rine is not effective at killing chlorine-resistant microbes such as *Giardia, Cryptosporidium* and *Bacillus* (Forsyth et al., 2013; Zhou et al., 2014). Ultraviolet (UV) disinfection can compensate for this defect, but it has the shortcoming of no continuous disinfection ability (Cheng et al., 2020; Zhu et al., 2014; Luo et al., 2020). Hence, the synergistic UV/Cl_2 process is often used to achieve a multiple-barrier disinfection and maintain residual protection. A series of free radical chain reactions occurs involving hydroxyl radical ($HO^{\bullet}$), chlorine radical ($Cl^{\bullet}$), oxygen radical ($O^{\bullet-}$) and hydroxyl- chloride radical ($ClHO^{\bullet-}$) (Eqs. (1)–(5)) (Watts and Linden, 2007; Chan et al., 2012).

$$HOCl \rightarrow H^{+}+ClO^{-} \quad (1)$$

$$HOCl+h\nu \rightarrow HO^{\bullet}+Cl^{\bullet} \quad (2)$$

$$OCl^{-}+h\nu \rightarrow O^{\bullet-}+Cl^{\bullet} \quad (3)$$

$$O^{\bullet-}+H_2O \rightarrow HO^{\bullet}+HO^{-} \quad (4)$$

$$Cl^{\bullet}+HO^{-} \rightarrow ClHO^{\bullet-} \quad (5)$$

Nowadays, the formation of nitrogenous disinfection byproducts (N-DBPs) has attracted much attention owing to their higher toxicity than carbonaceous disinfection byproducts (C-DBPs) (Muellner et al., 2007). Halonitromethanes (HNMs) is a typical class of N-DBPs, containing a nitro group and halogens on α-carbon. In mammalian cell experiments in vitro, the cytotoxicity of HNMs was several orders of magnitude higher than trihalomethanes (THMs) and haloacetic acids (HAAs) (Wagner and Plewa, 2017). Given this, HNMs were listed as the priority control disinfection byproducts (DBPs) by the Environmental Protection Agency of the United States (Woo et al., 2002). Nine HNMs species were identified including chloronitromethane (MCNM), bromochloro- nitromethane (BCNM), bromodichloronitromethane (BDCNM), bromonitromethane (MBNM), dichloronitromethane (DCNM), dibromonitromethane (DBNM), tribromo- nitromethane (TBNM), dibromochloronitromethane (DBCNM), trichloronitromethane (TCNM). Therefore, brominated HNMs are more cytotoxic and genotoxic than their chlorinated analogues, especially DBNM (Plewa et al., 2004).

Amines are widespread in aqueous environments with concentrations up to several mg/L, which derive from natural as well as industrial sources (Yu et al., 2002; Poste et al., 2014). Such hydrophilic nitrogenous compounds are often important precursors of HNMs during chlorination and chloramination (Chu et al., 2016; Zhou et al., 2021). In generally, it is believed that the formation pathway of HNMs from amines involves *N*-chlorination, *N*-nitration, α-C-chlorination and dealkylation (Joo and Mitch, 2007; Han et al., 2019). Nevertheless, to our best knowledge, there is no report revealing the transformation mechanisms of amines to HNMs during UV/Cl_2 disinfection.

Bromide ion (Br^{-}) is a common component of water matrix and can be oxidized to free bromine (HOBr/OBr^{-}) during chlorination (Eqs. (6) and (7)) (Heeb et al., 2014; Hu et al., 2016). HOBr is much more reactive toward amines than HOCl (Criquet et al., 2015). Under the UV irradiation, HOBr can be converted to active bromine radicals, such as bromine radical ($Br^{\bullet}$), oxybromine radical ($BrO^{\bullet}$) hydroxylbromide radical ($BrHO^{\bullet-}$) and dibromine radical ($Br_2^{\bullet}$) (Eqs. (8)–(12)) (Fang et al., 2014). Meanwhile, Br^{-} can also react with $Cl^{\bullet}$ to produce bromochloride radical ($ClBr^{\bullet-}$) (Eq. (13)) (Cheng et al., 2018). Sivey et al. (2013) demonstrated that the intrinsic brominating reactivity increased in the order of HOBr < Br_2 < BrCl and demonstrated that species other than HOBr affected bromination rates under typical chlorination conditions in drinking water or wastewater. It is expected that the formation of HNMs from amines will be greatly affected by the complex active bromine radicals formed in the UV/Cl_2 process.

$$HOCl + Br^{-} \rightarrow HOBr + Cl^{-} \quad (6)$$

$$OCl^{-}+Br^{-} \rightarrow OBr^{-}+Cl^{-} \quad (7)$$

$$HOBr+h\nu \rightarrow HO^{\bullet}+Br^{\bullet} \quad (8)$$

$$HOBr + HO^{\bullet} \rightarrow BrO^{\bullet}+H_2O \quad (9)$$

$$HO^{\bullet}+Br^{-} \rightarrow BrHO^{\bullet-} \quad (10)$$

$$Br^{\bullet} + Br^{-} \rightarrow Br_2^{\bullet-} \quad (11)$$

$$BrHO^{\bullet-} + Br^{-} \rightarrow Br_2^{\bullet-} + HO^{-} \quad (12)$$

$$Cl^{\bullet}+Br^{-} \rightarrow BrCl^{\bullet-} \quad (13)$$

In this paper, methylamine was selected as a precursor to study the formation of HNMs in the presence of Br^{-} during UV/Cl_2 disinfection. Emphatically, the formation mechanism of HNMs were explored by identifying the generation of intermediates and monitoring the change of chlorine, bromine and nitrogen form. The effect of pH value and Cl_2:Br^{-} ratio were also investigated in detail. Finally, two water samples collected from a water supply plant and a wastewater treatment plant were filtered and tested to verify the laboratory findings. This study helps to understand the formation of HNMs, especially brominated species, with UV/Cl_2 process adopted as a disinfection technique.

1. Materials and methods

1.1. *Chemical reagents*

All chemicals were of analytical grade or higher. Nine HNMs were obtained from Quality Control Chemicals (Newark, USA). Sodium hypochlorite, sodium thiosulfate and sodium bromide were purchased from Sinopharm Chemical Reagent (Shanghai, China). *N*,*N*-diethyl-*p*-phenylenediamine (DPD) was obtained from Chengdu Jiuding Chemical Technology (China). Methylamine hydrochloride, ammonium sulfate, methyl *tert*-butyl ether (MTBE) and ferrous ammonium sulphate (FAS) were purchased from Aladdin (Shanghai, China). Two real waters were collected from a water supply plant and wastewater treatment plant in Nanjing City (China) and filtered through 0.45-μm membrane filters. The water quality of the two real waters were shown in Appendix A Table S1.

1.2. *Experimental system*

The schematic diagram of self-made photochemical reactor is shown in Appendix A Fig. S1, which is a double-layer cylindrical quartz vessel with an inner diameter of 10 cm and a height of 15 cm. A low-pressure mercury lamp (254 nm, 15 W) was addressed in the center of cylinder. The photon fluence rate received in the solution was 1.45×10^{-4} einstein/(L•sec) measured by iodide-iodate chemical actinometry (Bolton et al., 2011). The effective path length was measured by the photolysis kinetics of dilute hydrogen peroxide, with a value of 3.05 cm (Crittenden et al., 1999). Correspondingly, the average fluence rate ($E_p{}^0$) was calculated to be 2.1 mW/cm^2 (Appendix A Text S1). The reactor was equipped with a water circulation system to maintain a steady reaction temperature (22 ± 2°C).

In the basic experiments, reaction solution (500 mL) was buffered with phosphate (20 mmol/L) at pH 7.0. To apparently observe the formation of HNMs, Br^- concentration, Cl_2 dose, and methylamine content were amplified synchronously to 4.0 mg/L, 20 mg/L and 30 mg/L, by a factor of about 4. After preselected times, water samples were quickly filtered through 0.22-μm membrane and then excess sodium thiosulfate was immediately spiked to quench residual oxidants for the quantification of total dissolved nitrogen (TDN), ammonia nitrogen (NH_4^+-N), nitrite nitrogen (NO_2^--N) and nitrate nitrogen (NO_3^--N). The concentration of dissolved organic nitrogen (DON) was calculated by subtracting the concentrations of NH_4^+-N, NO_2^--N and NO_3^--N from the content of TDN. For HNMs analysis, ammonium sulfate was employed as a quencher and the samples were extracted by with MTBE (USEPA, 1995; Kristiana et al., 2014).

1.3. *Analytical methods*

HNMs were quantified by an Agilent 6890N gas chromatography (GC) equipped with an electron capture detection (ECD) and DB-1 column (5.0 μm, 30 m × 0.32 mm). The instrumental conditions were shown below: 1.0 mL/min of nitrogen carrier gas velocity, 2.0 μL of injection volume (splitless), 235 and 280°C of injector temperature and detector temperature; the oven temperature of 50°C for 5 min, linearly to 140°C in 9 min, and finally linearly to 280°C in 7 min. The standard curves were shown in Appendix A Table S2. The intermediates were analyzed by a gas chromatograph- quadrupole mass spectrometer (GC-MS, Agilent 7890A GC, 5975 MS) with a HP-5m separation column (30 m × 0.25 mm, 0.25 μm). The conditions of GC were as follows: 1.0 μL of injection volume, 1.0 mL/min of helium carrier gas velocity; 300 and 280°C of injector and detector temperature; the oven temperature of 40°C for 2 min, ramped to 300°C at 40°C/min and finally held for 5 min. The MS was operated in the total ion chromatogram mode and selected ion monitoring mode.

TDN concentration was determined by a Shimadzu TOC-V_{CSH} analyzer. NH_4^+-N was analyzed by the salicylic acid–hypochlorous acid salt colorimetric method. NO_2^-, NO_3^- and Br^- concentration was analyzed by a Dionex ICS-2000 ion chromatography with an eluent flow rate of 1.0 mL/min (KOH, 20 mmol/L). Free and total chlorine and bromine were analyzed by DPD-FAS titration (Shang et al., 2000).

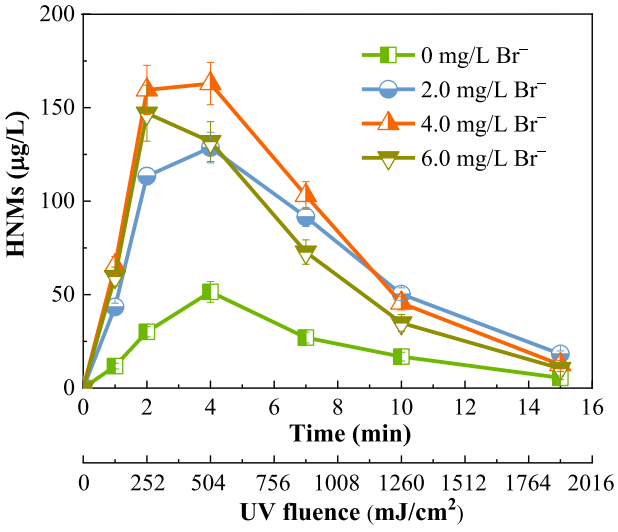

Fig. 1 – Total formation of halonitromethanes (HNMs) in the presence of bromide (Br^-). Experimental conditions: $[methylamine]_0$ = 30 mg/L, $[chlorine]_0$ = 20 mg/L Cl_2, pH = 7. Error bars represent the relative percent differences (n = 2).

2. Results and discussion

2.1. *Formation of HNMs in the presence of Br^-*

Fig. 1 illustrates the formation of HNMs in the absence and presence of Br^- during UV/Cl_2 disinfection. The HNMs yield increased first and then decreased whether Br^- was present or not. The dynamic evolution of HNMs yield was caused collectively by its enhanced formation in the UV/Cl_2 process and photolysis under the UV irradiation (Chen et al., 2013; Chen et al., 2017; Deng et al., 2014; Dong et al., 2017). In addition, the oxidation of free radicals was also a factor in the decline of HNMs yield (Mezyk et al., 2006; Fang et al., 2013). The maximum yield of HNMs substantially increased by 216.7% when Br^- concentration increased from 0.0 to 4.0 mg/L, while slightly decreased by 9.7% as Br^- concentration further increased to 6.0 mg/L. Evidently, an excessively high concentration of Br^- led to the maximum yield of HNMs in advance. The inflection point of HNMs yield appeared at an UV fluence of 252 mJ/cm^2 (i.e., 2.0 min reaction) when Br^- concentration was 6.0 mg/L, but it occurred at an UV fluence of 504 mJ/cm^2 (i.e., 4.0 min reaction) when Br^- concentration was less than 4.0 mg/L. The above results can be ascribed to two opposite aspects: on the one hand, high concentrations of Br^- increased the generation of bromine species with high reactivity towards methylamine, favoring the substitution of bromine and thus promoting the formation of brominated HNMs; on the other hand, the dissociation energy of carbon-halogen (C–X) bond decreases as the halogen shifts from chlorine to bromine. The lower dissociation energy of C–Br bond (280 kJ/mol) than C–Cl bond (328 kJ/mol) indicates that the brominated HNMs were more easily decomposed by direct UV photolysis or indirect radical oxidation than their chlorinated analogues (Hu et al., 2019). In a study of Huang et al. (2019), UV irradiation sharply reduced the total organic halogen con-

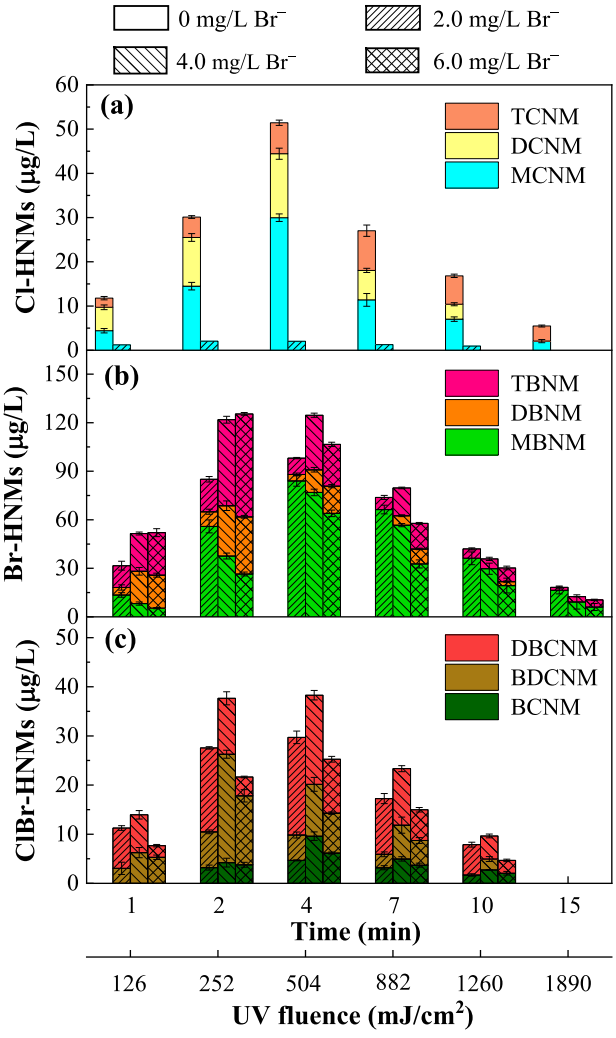

Fig. 2 – Formation of individual HNMs in the presence of Br^-. Experimental conditions: $[methylamine]_0$ = 30 mg/L, $[chlorine]_0$ = 20 mg/L Cl_2, pH = 7. Error bars represent the relative percent differences (n = 2).

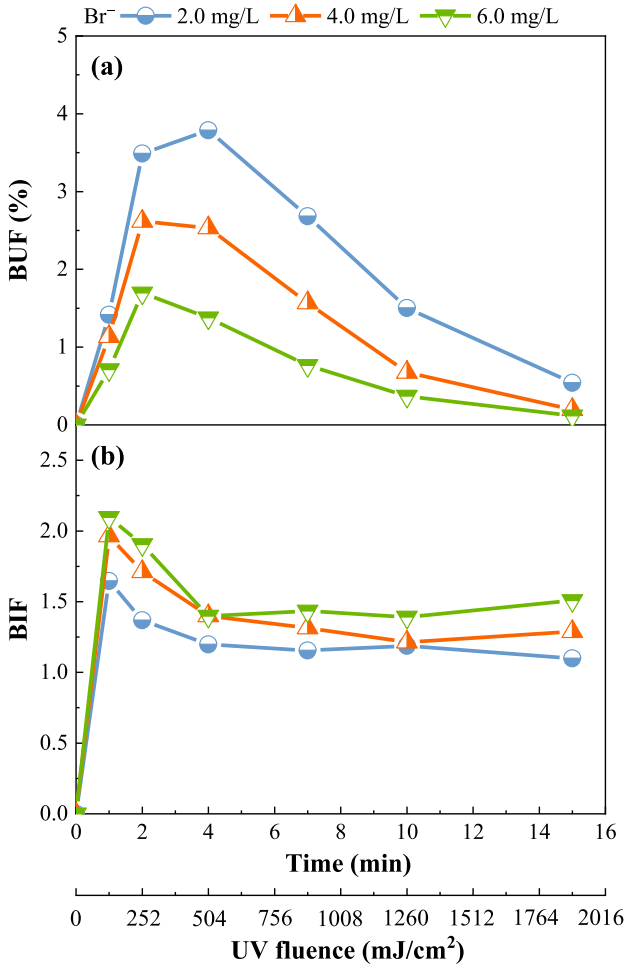

Fig. 3 – Bromine utilization factor (BUF) and bromine incorporation factor (BIF) values of HNMs. Experimental conditions: $[methylamine]_0$ = 30 mg/L, $[chlorine]_0$ = 20 mg/L Cl_2, pH = 7.

tent in chlorinated waters, in which the removal rate of total organic chlorine was in a range of 25.9%–53.6% and that of total organic bromine was about 60% at an UV fluence of 2400 mJ/cm^2.

To study the species distribution, HNMs are classified into three groups: Cl-HNMs, including MCNM, DCNM and TCNM; ClBr-HNMs, including BCNM, DCBNM and DBCNM; and Br-HNMs, including MBNM, DBNM and TBNM. As shown in Fig. 2, the species of HNMs shifted from Cl-HNMs to ClBr-HNMs and Br-HNMs with the increase of Br^- concentration. The Cl-HNMs formation became almost invisible when Br^- concentration achieved 2.0 mg/L (Fig. 2a). Elsewise, bromine utilization factor (BUF) and bromine incorporation factor (BIF) were calculated to study the impact of Br^- on the speciation of HNMs (Appendix A Text S2). BUF refers to the percentage of Br^- that is utilized in forming Br-DBPs, and BIF is used as an index to describe the proportion of Br-DBPs that is partially or totally substituted by bromine. As the reaction proceeded, the BUF value increased first and then decreased gradually, implying that bromine substitution and elimination achieved equilibrium at a certain UV fluence (or reaction time) (Fig. 3a). However, the BIF value decreased dramatically when the UV fluence was above 126 mJ/cm^2 (i.e., after 1.0 min reaction) (Fig. 3b). In the presence of Br^- (> 2.0 mg/L), Br-HNMs were the primary species, while ClBr-HNMs were the minorities (Fig. 2b and 2c). Thus, the decrease of BIF value was mainly caused by the shift from TBNM and DBNM to MBNM, making the latter become the dominant species of Br-HNMs. Such a shift can be interpreted as the reduced production of reactive bromine species (the sum of free bromine and active bromine radicals) with the chlorine consumption, and the decomposition of C–Br bond by direct UV photolysis or indirect radical oxidation. As expected, the maximum BIF value increased with the increase of Br^- concentration since more active bromine species was produced. The maximum BIF value increased from 1.6 to 2.1 when Br^- concentration increased from 2.0 to 6.0 mg/L. In contrast, the maximum BUF value decreased from 3.8% to 1.7%, implying that the utilized Br^- did not increase in proportion to its initial concentration.

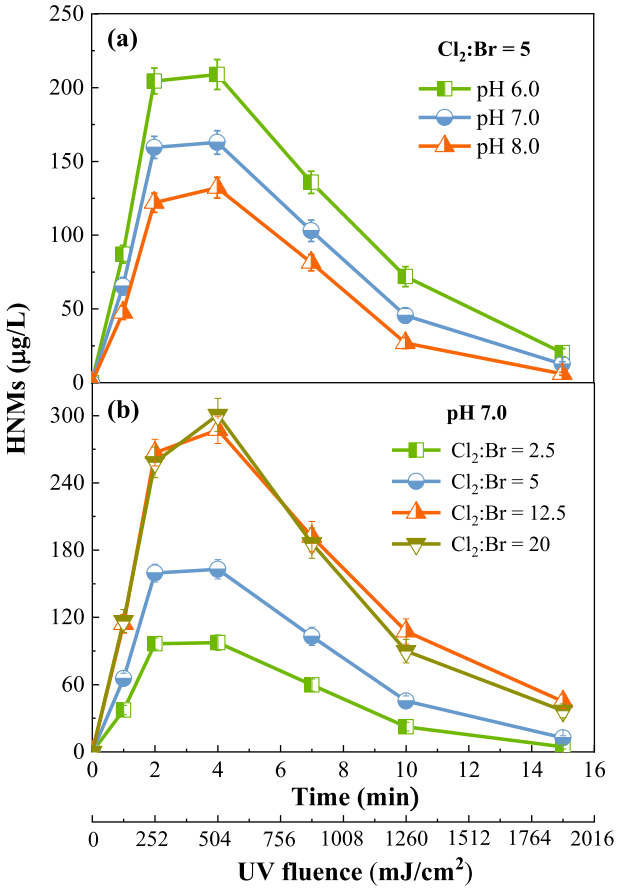

Fig. 4 – Impact of pH value and Cl_2:Br ratio on the formation of HNMs. Experimental conditions: [methylamine]$_0$ = 30 mg/L, [Br^-]$_0$ = 4.0 mg/L. Error bars represent the relative percent differences (n = 2).

2.2. *Impact factors*

2.2.1. *Effect of pH*

The reaction pH was set in the range of 6.0–8.0 to study its effect on the formation of HNMs from methylamine. The HNMs yield maximized at an UV fluence of 504 mJ/cm^2 (i.e., 4.0 min reaction) at all investigated pH values (Fig. 4a). The maximum yield decreased by 36.7% as pH value increased from 6.0 to 8.0, which indicates that the increase of pH was unfavorable to the formation of HNMs. The dissociation constant (pK_a) values of HOCl and HOBr were 7.5 and 8.6, respectively. At pH 6.0, HOCl and HOBr are the dominant species, while OCl^- and OBr^- account for more than 60% and 15% of free chlorine and bromine, respectively, at pH 8.0 (Liu et al., 2012). First, the deprotonation process at a higher pH weakened the substitution reaction of free bromine and chlorine with methylamine. Second, the apparent quantum yield (Φ) and molar absorption coefficient (ε) of OBr^- (Φ_{OBr-}, 0.43 mol/einstein; ε_{OBr-}, 28 L/(mol•cm)) are lower than those of HOBr (Φ_{HOBr}, 0.75 mol/einstein; ε_{HOBr} = 77 L/(mol•cm)), at 254 nm at an ambient temperature (Zhang et al., 2020). This rule is also applicable to HOCl and OCl^- (Yeom et al., 2021). Thereby, the deprotonation can also reduce the production of active chlorine and bromine radicals under the UV irradiation. Moreover, the oxidation capacity of radicals generally decreased with the increase of pH value.

In the presence of Br^- (4.0 mg/L), the Cl-HNMs formation was entirely invisible at all pH values. The formation of Br- and ClBr-HNMs were more conducive to occur under an acidic condition (Appendix A Fig. S2). The BUF value showed the same trend (Appendix A Fig. S3a). On the one hand, the deprotonation of HOCl reduced the production of HOBr, and then the deprotonation of HOBr weakened its substitution reaction. On the other hand, the reducing production and oxidation capacity of reactive bromine species also retarded the substitution of bromine onto methylamine. As shown in Appendix A Fig. S3b, the variation of pH value had no significant influence on the BIF value, which means that the effect of pH on the substitution of chlorine was similar to that of bromine.

2.2.2. *Effect of Cl_2:Br^- ratio*

The impact of Cl_2:Br^- ratio on the HNMs formation was investigated in the range of 2.5–20. As shown in Fig. 4b, the maximum yield of HNMs increased by 195% when Cl_2:Br^- ratio increased from 2.5 to 12.5, while no apparent difference was observed as Cl_2:Br^- ratio further increased to 20. The increase of free chlorine not only directly led to the increase of reactive chlorine species, but also resulted in the increase of reactive bromine species indirectly due to the accelerated production of free bromine. However, the reactive chlorine and bromine species produced may achieve saturation relative to methylamine when free chlorine was in excess.

As shown in Appendix A Fig. S4, the maximum yield of Cl-HNMs and ClBr-HNMs increased, while that of Br-HNMs increased first and then decreased with the increase of Cl_2:Br^- ratio. Concretely, the Cl-HNMs formation was not observed until Cl_2:Br^- ratio reached 12.5, and its maximum yield increased by 37.0% when Cl_2:Br^- ratio further increased to 20. The maximum yield of ClBr-HNMs increased by 4.6 times when Cl_2:Br^- ratio increased from 2.5 to 20. For Br-HNMs, the maximum yield increased by 82.9% and then decreased by 21.3% as Cl_2:Br^- ratio successively increased from 2.5 to 12.5 and 20, respectively. The BUF value achieved the maximum at a Cl_2:Br^- ratio of 12.5, but the BIF value remained relatively higher at Cl_2:Br^- ratios of 2.5 and 5 (Appendix A Fig. S5). When free chlorine was scare, most of them participated in the oxidation of Br^- to form free bromine and then generate active bromine radicals. With the increase of free chlorine, reactive chlorine species competed with reactive bromine species for methylamine to form chlorinated HNMs (including Cl-, and ClBr-HNMs), which led to the decline of BIF value. Such a phenomenon is similar to that found in a study by Hua and Reckhow (2012), in which the BIF value was evaluated during chlorination and chloramination. As described above, the increase of free chlorine also induced the increase of reactive bromine species, resulting in the increase of BUF value. Nevertheless, the competition may also cause the decline of BUF value when free chlorine was in excess. Moreover, excess free chlorine may form a large number of $HO^•$, which can oxidize the produced free bromine to bromate, or eliminate the bromine from brominated HNMs (Br- and Cl-Br-HNMs).

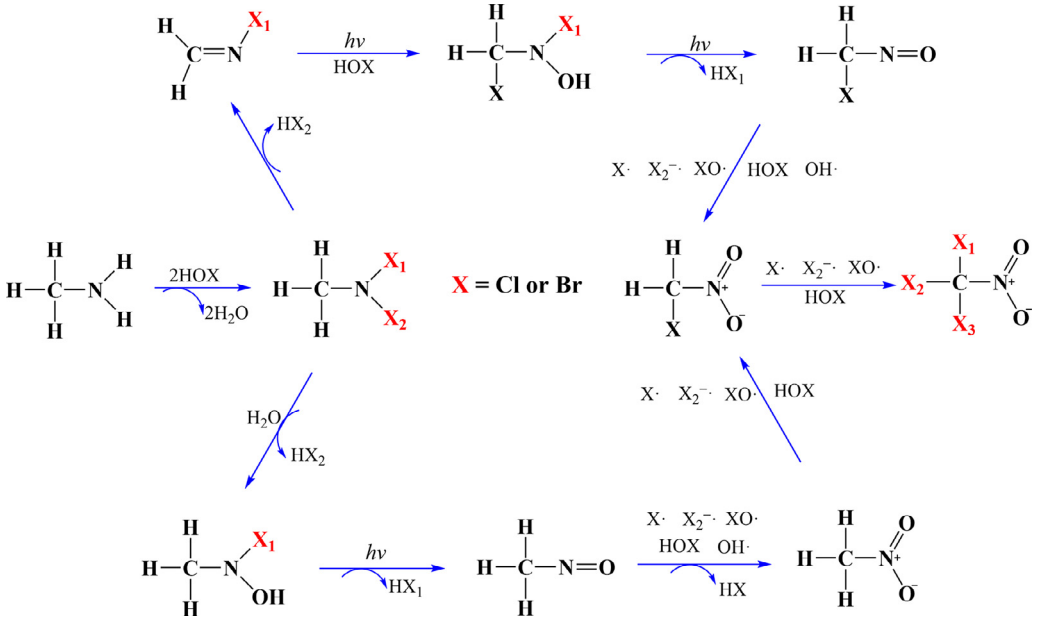

Fig. 5 – Possible reaction mechanism of the HNMs formation. Experimental conditions: [methylamine]$_0$ = 30 mg/L, [chlorine]$_0$ = 20 mg/L Cl_2, [Br^-]$_0$ = 4.0 mg/L, pH = 7.

2.3. *Possible reaction mechanisms*

Fig. 5 presents the possible reaction mechanisms of reactive chlorine and bromine species with methylamine. The hydrogens in the amino group were easily chlorinated or brominated to form organochloramines or organobromoamines, respectively (Abia et al., 1998; Lee and Westerhoff, 2009; How et al., 2017). As illustrated in Fig. 6a, free chlorine and bromine were rapidly converted to combined chlorine and bromine, which also revealed that the first reaction step was halogenation (Joo and Mitch, 2007; Yang et al., 2012; Ding et al., 2013). The combined chlorine and bromine decreased as the reaction proceeded, which indicates that organochloramines and organobromoamines occurred further conversion during UV/Cl_2 disinfection. The concentration of NH_4^+-N always increased, while that of NO_3^--N increased first and then decreased with the increase of UV fluence (reaction time) (Fig. 6b). NO_2^--N was not detected, possibly since reaction solution maintained a strong oxidation capacity. After calculation, the DON content decreased as the reaction proceeded. It is inferred that the C-N bond in organochloramines or organobromoamines was ruptured, and inorganic nitrogen was released into solution. A powerful evidence is that bromoform was detected during the reactions (Appendix A Fig. S6).

In a study by Joo and Mitch (2007), dimethylchloramine underwent oxidation and elimination reactions during chlorination. Analogously, organochloramines and organobromoamines may also occur two reaction pathways in the formation of HNMs. In the oxidation pathway, the N-X bond (X = Cl or Br) underwent heterolysis with two water molecules to produce CH_3N^+X/X^- ion pairs, while another water molecule acted as a nucleophile to attack the N^+ site to form *N*-halogen-*N*-methylhydroxylamine (Joo and Mitch, 2007; Han et al., 2019), which can be transformed to nitrosomethane through the elimination of hydrogen halide. Nitrosomethane was unstable, and can be oxidized to generate nitromethane and then halogenated to produce HNMs. Due to the fact that the substitution capacity of reactive bromine species was higher than reactive chlorine species (Heeb et al., 2017; Liu et al., 2018), nitromethane was more likely to occur bromination to form brominated HNMs (Br-HNMs and ClBr-HNMs) when Br^- existed. In the elimination pathway, organochloramines and organobromoamines may undergo the elimination of hydrogen chloride and hydrogen bromide, respectively, to form *N*-chloromethanimine and *N*-bromomethanimine (Yang et al., 2012). The C=N bond underwent addition reaction to form *N*-chloro-*N*-(chloromethyl)hydroxylamine, *N*-bromo-*N*-(chloromethyl)hydroxylamine, *N*-chloro-*N*-(bromomethyl)hydroxylamine and *N*-bromo-*N*-(bromomethyl)hydroxylamine (Joo and Mitch, 2007). Subsequently, the hydroxylamines were converted to monochloro-nitrosomethane and monobromo- nitrosomethane by the second elimination of hydrogen chloride and hydrogen bromide (Han et al., 2019). Similar to the oxidation pathway, monochloro-nitrosomethane and monobromo-nitrosomethane were then transformed to monochloro-nitromethane and monobromo-nitromethane, respectively, which were halogenated to produce various HNMs (Appendix A Fig. S6).

2.4. *HNMs formation in real waters containing methylamine*

Two filtered real waters were collected from a wastewater treatment plant (TW) and water supply plant (SW) to verify the formation laws of HNMs in pure water (PW) during UV/Cl_2 disinfection. The water quality of TW and SW was shown in Appendix A Table S1. The formation of HNMs in

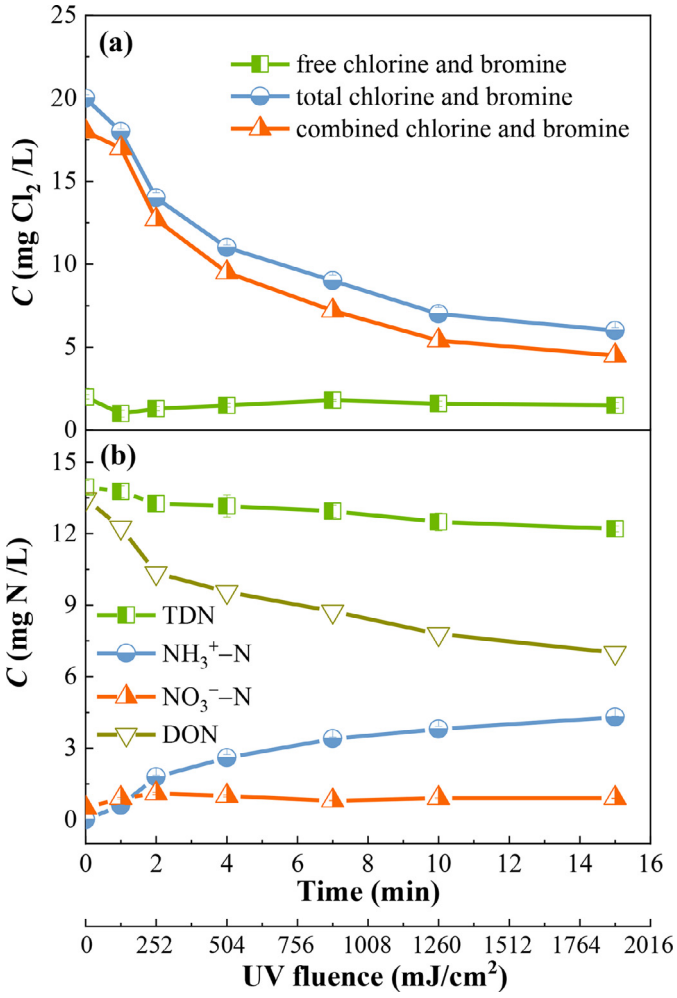

Fig. 6 – Transformation of oxidant (a) and nitrogen (b) species. Experimental conditions: $[methylamine]_0$ = 30 mg/L, $[chlorine]_0$ = 20 mg/L Cl_2, $[Br^-]_0$ = 4.0 mg/L, pH = 7. Error bars represent the relative percent differences (n = 2).

TW and SW also increased first and then decreased, which was the same as that in PW. The inflection points in the three waters appeared at an UV fluence of 504 mJ/cm^2 (i.e., 4.0 min reaction) (Fig. 7). Compared with PW, the maximum yield in TW was much higher, but that in SW was similar, with values of 287.3, 388.1, and 245.5, respectively. All the three species also presented the same trend (Appendix A Fig. S7). The results can be mainly attributed to the higher content of dissolved organic carbon in TW (83.0 mg/L), which provided more precursors for the HNMs formation. Additionally, the BUF value also achieved the maximum in TW, indicating that more reactive bromine species reacted with the organic matter in water to form Br- and ClBr-HNMs (Appendix A Fig. S8). However, the BIF value was slightly lower in TW, which demonstrates that the incorporation of bromine into the aqueous organic matter did not catch up with that of chlorine.

3. Conclusions

In this study, methylamine was selected as a precursor to study the formation of HNMs in the presence of Br^- during UV/Cl_2 disinfection. Based on the experimental data, the following conclusions were drawn:

- The maximum yield of HNMs reached the maximum with a Br^- concentration of 4.0 mg/L. An excessively high concentration of Br^- led to the maximum yield of HNMs in advance. The maximum value of BIF increased, while that of BUF decreased with the increase of Br^- concentration.
- The maximum yield of HNMs decreased with the increase of pH value due to the deprotonation process. The BUF value remained relatively higher under an acidic condition, while pH value had no significant influence on the BIF value.
- The maximum yield of HNMs and value of BUF maximized at a Cl_2:Br^- ratio of 12.5, whereas the BIF value remained relatively higher at low Cl_2:Br^- ratios.
- The amino group were first halogenated, and then released into reaction solution as inorganic nitrogen by the rupture of C-N bond or transformed to nitro group by oxidation and elimination pathways.
- The maximum yield of HNMs in TW was much higher than those in SW and PW due to the higher content of dissolved organic carbon. The BUF value increased, while BIF slightly decreased when switching from PW to TW.

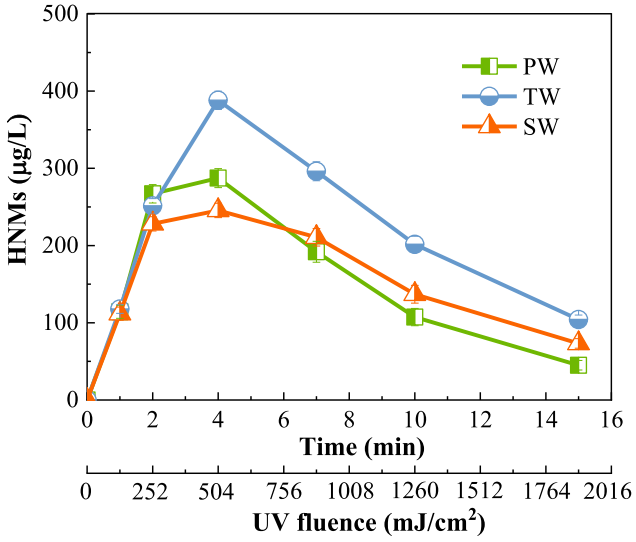

Fig. 7 – Total formation of HNMs in two filtered real waters containing methylamine. Experimental conditions: [methylamine]$_0$ = 30 mg/L, [chlorine]$_0$ = 50 mg/L Cl_2, [Br^-]$_0$ = 4.0 mg/L, pH = 7. Error bars represent the relative percent differences (n = 2). PW: pure water; TW: wastewater treatment plant; SW, water supply plant.

Acknowledgments

This study was financially supported by the National Natural Science Foundation of China (Nos. 22076023, 21677032 and 51808496).

Appendix A Supplementary data

Supplementary material associated with this article can be found, in the online version, at doi:10.1016/j.jes.2021.12.031.

REFERENCES

Abia, L., Armesto, X.L., Canle, M.L., García, M.V., Santaballa, J.A., 1998. Oxidation of aliphatic amines by aqueous chlorine. Tetrahedron 54, 521–530.

Bolton, J.R., Stefan, M.I., Shaw, P.S., Lykke, K.R., 2011. Determination of the quantum yields of the potassium ferrioxalate and potassium iodide–iodate actinometers and a method for the calibration of radiometer detectors. J. Photoch. Photobio. A 222, 166–169.

Chan, P.Y., Gamal El-Din, M., Bolton, J.R., 2012. A solar-driven UV/Cl_2 advanced oxidation process. Water Res 46 (17), 5672–5682.

Chen, Y., Liang, J.F., Liu, L., Lu, X.Y., Deng, J.W., Pozdnyakov, I.P., et al., 2017. Photosensitized degradation of amitriptyline and its active metabolite nortriptyline in aqueous fulvic acid solution. J. Environ. Qual. 46 (5), 1081–1087.

Chen, Y., Liang, Q., Zhou, D.N., Wang, Z.P, Tao, T., Zuo, Y.G., 2013. Photodegradation kinetics, products and mechanism of timolol under simulated sunlight. J. Hazard. Mater. 252, 220–226.

Cheng, Y., Song, R.Q., Wu, K., Peng, N., Yang, M., Luo, J., et al., 2020. The enhanced visible-light-driven antibacterial performances of PTCDI-PANI (Fe (III)-doped) heterostructure. J. Hazard. Mater. 383, 121166.

Cheng, S.S., Zhang, X.R., Yang, X., Shang, C., Song, W.H., Fang, J.Y., et al., 2018. The multiple role of bromide ion in PPCPs degradation under UV/chlorine treatment. Environ. Sci. Technol. 52, 1806–1816.

Chu, W.H., Chu, T.F., Bond, T., Du, E.D., Guo, Y.Q., Gao, N.Y., 2016. Impact of persulfate and ultraviolet light activated persulfate preoxidation on the formation of trihalomethanes, haloacetonitriles and halonitromethanes from the chlor(am)ination of three antibiotic chloramphenicols. Water Res 93, 48–55.

Crittenden, J.C., Hu, S.M., Hand, D.W., Green, S.A., 1999. A kinetic model for H_2O_2/UV process in a completely mixed batch reactor. Water Res 33, 2315–2328.

Criquet, J., Rodriguez, E.M., Allard, S., Wellauer, S., Salhi, E., Joll, C.A., et al., 2015. Reaction of bromine and chlorine with phenolic compounds and natural organic matter extracts – electrophilic aromatic substitution and oxidation. Water Res 85, 476–486.

Deng, L., Huang, C.H., Wang, Y.L., 2014. Effects of combined UV and chlorine treatment on the formation of trichloronitromethane from amine precursors. Environ. Sci. Technol. 48, 2697–2705.

Ding, C.S., Zou, B.W., Miao, J., Fu, Y.P., Shen, J.C., 2013. Formation process of nitrogenous disinfection byproduct trichloronitromethane in drinking water and its influencing factors. Environ. Sci. 34, 3113–3118.

Dong, H.Y., Qiang, Z.M., Hu, J., Qu, J.H., 2017. Degradation of chloramphenicol by UV/chlorine treatment: kinetics, mechanism and enhanced formation of halonitromethanes. Water Res 121, 178–185.

Fang, J.Y., Ling, L., Shang, C., 2013. Kinetics and mechanisms of pH-dependent degradation of halonitromethanes by UV photolysis. Water Res 47, 1257–1266.

Fang, J.Y., Fu, Y., Shang, C., 2014. The roles of reactive species in micropollutant degradation in UV/free chlorine system. Environ. Sci. Technol. 48, 1859–1868.

Forsyth, J.E., Zhou, P., Mao, Q.X., Asato, S.S., Meschke, J.S., Dodd, M.C., 2013. Enhanced inactivation of *Bacillus subtilis* spores during solar photolysis of free available chlorine. Environ. Sci. Technol. 47, 12976–12984.

Han, C.X., Zhao, H.Y., Dong, M., Liu, Y.D., Zhong, R.G., 2019. The formation mechanism of chloropicrin from methylamine during chlorination: a DFT study. Environ. Sci. Proc. Imp. 21, 761–770.

Heeb, M.B., Criquet, J., Zimmermann-Steffens, S.G., von Gunten, U., 2014. Oxidative treatment of bromide-containing waters: formation of bromine and its reactions with inorganic and organic compounds – a critical review. Water Res 48, 15–42.

Heeb, M.B., Kristiana, I., Trogolo, D., Arey, J.S., von Gunten, U., 2017. Formation and reactivity of inorganic and organic chloramines and bromamines during oxidative water treatment. Water Res 110, 91–101.

Hu, J., Qiang, Z.M., Dong, H.Y., Qu, J.H., 2016. Enhanced formation of bromate and brominated disinfection byproducts during chlorination of bromide-containing waters under catalysis of copper corrosion products. Water Res 98, 302–308.

Hu, J., Wang, C., Ye, Z., Dong, H.Y., Li, M.K., Chen, J.M., et al., 2019. Degradation of iodinated disinfection byproducts by VUV/UV process based on a mini-fluidic VUV/UV photoreaction system. Water Res 158, 417–423.

Huang, W.C., Du, Y., Liu, M., Hu, H.Y., Wu, Q.Y., Chen, Y., 2019. Influence of UV irradiation on the toxicity of chlorinated water to mammalian cells: toxicity drivers, toxicity changes and toxicity surrogates. Water Res 165, 115024.

How, Z.T., Kristiana, I., Busetti, F., Linge, K.L., Joll, C.A., 2017. Organic chloramines in chlorine-based disinfected water systems: a critical review. J. Environ. Sci. 58, 2–18.

Joo, S.H., Mitch, W.A., 2007. Nitrile, aldehyde, and halonitroalkane formation during chlorination/chloramination of primary amines. Environ. Sci. Technol. 41, 1288–1296.
Kristiana, I., Lethorn, A., Joll, C., Heitz, A., 2014. To add or not to add: the use of quenching agents for the analysis of disinfection byproducts in water samples. Water Res 59, 90–98.
Lee, W., Westerhoff, P., 2009. Formation of organic chloramines during water disinfection – chlorination versus chloramination. Water Res 43, 2233–2239.
Liu, C., von Gunten, U., Croué, J.P., 2012. Enhanced bromate formation during chlorination of bromide-containing waters in the presence of CuO: catalytic disproportionation of hypobromous acid. Environ. Sci. Technol. 46, 11054–11061.
Liu, R.P., Tian, C., Hu, C.Z., Qi, Z.L., Liu, H.J., Qu, J.H., 2018. Effects of bromide on the formation and transformation of disinfection byproducts during chlorination and chloramination. Sci. Total. Environ. 625, 252–261.
Luo, Y.C., Feng, L., Liu, Y.Z., Zhang, L.Q., 2020. Disinfection byproducts formation and acute toxicity variation of hospital wastewater under different disinfection processes. Sep. Purif. Technol. 238, 116405.
Muellner, M.G., Wagner, E.D., McCalla, K., Richardson, S.D., Woo, Y.T., Plewa, M.J., 2007. Haloacetonitriles vs. regulated haloacetic acids: are nitrogen-containing DBPs more toxic? Environ. Sci. Technol. 41 (2), 645–651.
Mezyk, S.P., Helgeson, T., Cole, S.K., Cooper, W.J., Fox, R.V., Gardinali, P.R., et al., 2006. Free radical chemistry of disinfection-byproducts. 1. Kinetics of hydrated electron and hydroxyl radical reactions with halonitromethanes in water. J. Phys. Chem. A. 110, 2176–2180.
Plewa, M.J., Wagner, E.D., Jazwierska, P., Richardson, S.D., Chen, P.H., McKague, A.B., 2004. Halonitromethane drinking water disinfection byproducts: chemical characterization and mammalian cell cytotoxicity and genotoxicity. Environ. Sci. Technol. 38 (1), 62–68.
Poste, A.E., Grung, M., Wright, R.F., 2014. Amines and amine-related compounds in surface waters: a review of sources, concentrations and aquatic toxicity. Sci. Total. Environ. 481, 274–279.
Shang, C., Gong, W.L., Blatchley, E.R., 2000. Breakpoint chemistry and volatile byproduct formation resulting from chlorination of model organic-N compounds. Environ. Sci. Technol. 34, 1721–1728.
Sivey, J.D., Arey, J.S., Tentscher, P.R., Roberts, A.L., 2013. Reactivity of BrCl, Br_2, BrOCl, Br_2O, and HOBr toward dimethenamid in solutions of bromide plus aqueous free chlorine. Environ. Sci. Technol. 47, 1330–1338.
USEPA, 1995. Method 551.1: determination of chlorination disinfection byproducts, chlorinated solvents, and halogenated pesticides/herbicides in drinking water by liquid-liquid extraction and gas chromatography with electron capture detection. Cincinnati, Ohio, US.
Watts, M.J., Linden, K.G., 2007. Chlorine photolysis and subsequent OH radical production during UV treatment of chlorinated water. Water Res 41 (13), 2871–2878.
Wagner, E.D., Plewa, M.J., 2017. CHO cell cytotoxicity and genotoxicity analyses of disinfection by-products: an updated review. J. Environ. Sci. 58, 64–76.
Woo, Y.T., Lai, D., Mclain, J.L., Manibusan, M.K., Dellarco, V., 2002. Use of mechanism-based structure-activity relationships analysis in carcinogenic potential ranking for drinking water disinfection byproducts. Environ. Health Perspect. 110, 75–87.
Yang, X., Shen, Q.Q., Guo, W.H., Peng, J.F., Liang, Y.M., 2012. Precursors and nitrogen origins of trichloronitromethane and dichloroacetonitrile during chlorination/chloramination. Chemosphere 88, 25–32.
Yeom, Y.J., Han, J.R., Zhang, X.R., Shang, C., Zhang, T., Li, X.Y., et al., 2021. A review on the degradation efficiency, DBP formation, and toxicity variation in the UV/chlorine treatment of micropollutants. Chem. Eng. J. 424, 130053.
Yu, Z., Zhang, Q., Kraus, T.E.C., Dahlgren, R.A., Anastasio, C., Zasoski, R.J., 2002. Contribution of amino compounds to dissolved organic nitrogen in forest soils. Biogeochemistry 61, 173–198.
Zhang, X.W., Guo, K.H., Wang, Y.G., Qin, Q.D., Yuan, Z.X., He, J., et al., 2020. Roles of bromine radicals, HOBr and Br_2 in the transformation of flumequine by the UV/chlorine process in the presence of bromide. Chem. Eng. J. 400, 125222.
Zhou, P., Di Giovanni, G.D., Meschke, J.S., Dodd, M.C., 2014. Enhanced inactivation of *Cryptosporidium parvum* oocysts during solar photolysis of free available chlorine. Environ. Sci. Technol. Lett. 1, 453–458.
Zhou, Y.Y., Ye, Z.X., Huang, H., Liu, Y.D., Zhong, R.G., 2021. Formation mechanism of chloropicrin from amines and free amino acids during chlorination: a combined computational and experimental study. J. Hazard. Mater. 416, 125819.
Zhu, Y., Wang, H.B., Li, X.X., Hu, C., Yang, M., Qu, J.H., 2014. Characterization of biofilm and corrosion of cast iron pipes in drinking water distribution system with UV/Cl_2 disinfection. Water Res 60, 174–181.